




Research Article



Mechanical and microstructural properties of geopolymer mortars from meta-halloysite: effect of titanium dioxide TiO₂ (anatase and rutile) content

Hawa Mohamed^{1,2}  · Juvenal Giogetti Nemaleu Deutou² · Cyriaque Rodrigue Kaze¹ · Lynn M. Beleuk à Mougam² · Elie Kamseu^{2,3} · Uphie Chinje Melo¹ · Cristina Leonelli³

Received: 22 April 2020 / Accepted: 20 August 2020 / Published online: 27 August 2020
© Springer Nature Switzerland AG 2020

Abstract

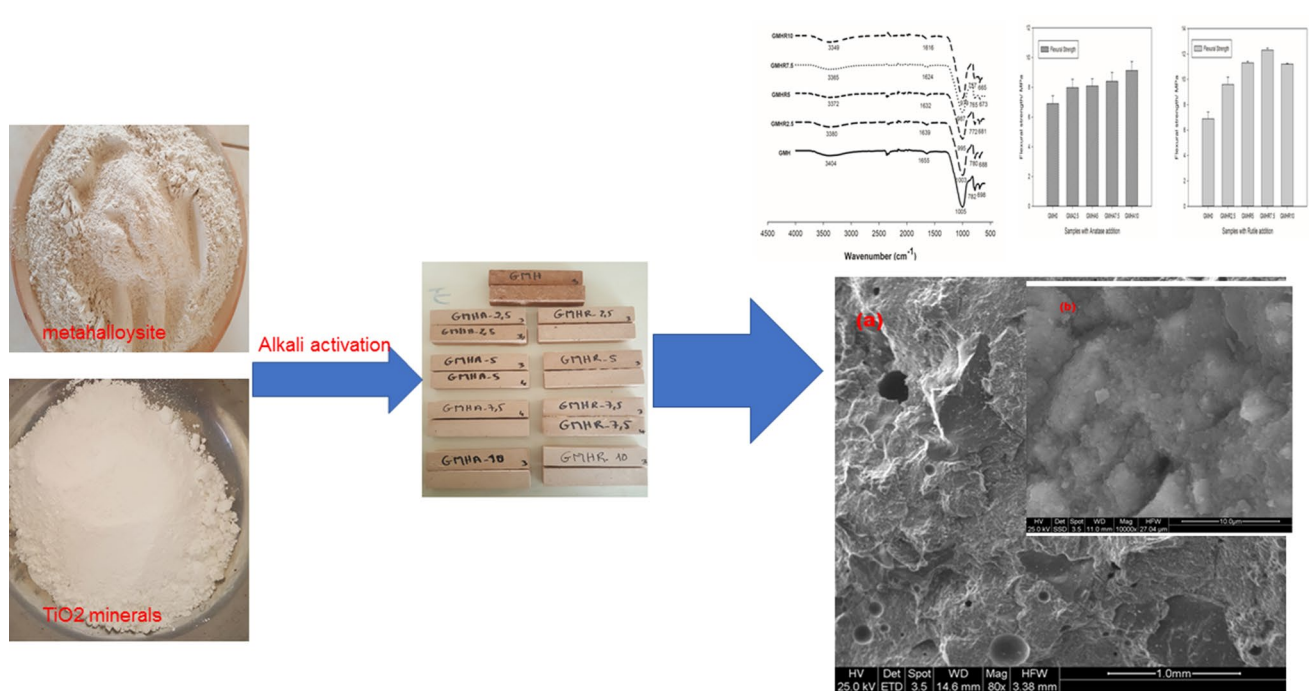
This study aimed to investigate the effect of Titanium Dioxide TiO₂ (anatase and rutile) on mechanical and microstructural properties of meta-halloysite based geopolymer mortars namely GMHA and GMHR series. Meta-halloysite received 2.5, 5.0, 7.5 and 10 wt% of anatase or rutile as addition before calcination and geopolymerization. The raw materials and the end products were characterized using XRD, FTIR, ESEM and MIP analyses. The flexural strength increases from 6.90 to 9.13 MPa and from 6.90 to 12.33 MPa for GMHA and GMHR series respectively. The cumulative pore volume decreases from 102.2 to 84.2 mm³ g⁻¹ and from 102.2 to 51.3 mm³ g⁻¹ for GMHA and GMHR products respectively. Both matrices present micrographs with very low capillaries pores and fractured surfaces that confirmed the enhancement of the mechanical properties. It was concluded that TiO₂ in both forms is beneficial for the reduction of porosity and densification of geopolymer matrices. Rutile enabled more compact and denser geopolymer structure compared to anatase. The aforementioned results showed the efficiency of both fine TiO₂ particles to improve the geopolymer network significant for its durability.

✉ Hawa Mohamed, mohamedhawa@hotmail.com; ✉ Elie Kamseu, kamseuelie2001@yahoo.fr | ¹Laboratory of Applied Inorganic Chemistry, Faculty of Science, University of Yaoundé I, P.O. Box 812, Yaoundé, Cameroon. ²Laboratory of Materials, Local Materials Promotion Authority, MINRESI/MIPROMALO, P.O. Box 2396, Yaoundé, Cameroon. ³Department of Engineering “Enzo Ferrari”, University of Modena and Reggio Emilia, Via P. Vicarelli 10, 41125 Modena, Italy.



SN Applied Sciences (2020) 2:1573 | <https://doi.org/10.1007/s42452-020-03396-5>

Graphic abstract



Keywords Meta-halloysite · Geopolymerization · Flexural strength · Titanium dioxide · Microstructure · Porosity

1 Introduction

Sustainable use of natural resources in the field of construction and building materials gained great attention in recent years. But in building industries, the most commonly used construction material is concrete. Ordinary Portland Cement (OPC) is conventionally used as the primary binder to produce concrete. However, the production of OPC contributes to 5–8% of global Carbon Dioxide (CO₂) emissions and releases of gases such as Nitrogen Oxide (NO_x) and Sulphur Oxide (SO_x) responsible for the greenhouse effect and acid rain [1]. The search for an innovative technology, new, sustainable and environmentally friendly materials is becoming a fundamental need. Geopolymers are green alternative to conventional cement and concrete produced from the OPC and to reduce the aforementioned problems of CO₂ emissions. Geopolymerization involves chemical reactions at low temperature between an amorphous to semi-crystalline aluminosilicate material and silicate solutions under highly alkaline conditions [2]. Its advantages are based on (a) low energy consumption, (b) low CO₂ emissions in the preparation process (curing at ambient temperature) [3], (c) the ability to withstand elevated temperature and fire, (d) acid and salt resistance [4] and (e) an extensive range of available

solid precursors such as metakaolin [5] and by products such as volcanic ash [6] and fly ash [7]. As geopolymers are seen as a material of future, its durability must be studied. Sustainability requires the development of stable, low-polluting products with low environmental impact.

Numerous nano-particles (SiO₂, Al₂O₃ and TiO₂) have been successfully used as improvement agent in terms of mechanical properties, microstructure as well as durability of binder, mortar and concretes [8]. Titanium dioxide, which is one of the mostly used, exhibits three polymorphs namely anatase, rutile and brookite. According to Pelaez et al. [9], anatase is made up of corner (vertice) sharing octahedra which form (001) planes resulting in a tetragonal structure. In rutile, the octahedral share edge at (001) planes to give a tetragonal structure and in brookite both edges and corners are shared to give and orthorhombic structure. Anatase type is more widely used because of its higher photocatalytic activity compared to the other types of TiO₂ [9–11]. Compared to other nano-particles, TiO₂ presents photocatalytic properties owing to its BET surface and pore size distribution. When introduced in cementitious matrices, it enhances their resistance to chemical attacks, allowing the degradation or deterioration of atmospheric pollutants like NO_x and SO_x, resulting in self-cleaning property [12–14]. Therefore, the presence

of TiO₂ particles in geopolymer network would act as wall protection to external attack related to their high surface area and fine particles that could extend the geopolymerization rendering the structure less permeable. Beside the depolluting ability of the materials added with TiO₂, the presence of titanium dioxide may also positively influence their mechanical properties. Recently, Guzmán-Aponte et al. [15] investigated the influence of TiO₂ on physico-mechanical properties of metakaolin-based geopolymer. The authors found that a percentage of up to 10% TiO₂ does not affect the mechanical properties of the geopolymer, although it does reduce the fluidity and setting times of the mixture indicating their participation into geopolymer reaction. Similar observation was reported by Duan et al. [16] who concluded through microstructural analysis uncovers that the addition of nano-TiO₂ promotes the formation of geopolymer and results in compact and dense microstructure with less cracks.

In this study, thermally treated Halloysite (700 °C) and a mix of potassium silicate and potassium hydroxide are used as source of aluminosilicate and alkaline activators respectively. According to the literature, geopolymers prepared using K-containing activators have better high-temperature resistant properties than those synthesized using Na-containing activators [15, 17, 18]. Lemougna et al. [19] also reported that the use of KOH in geopolymer synthesis improves the degree of polycondensation and tends to produce stronger matrixes resulting in high strength. From the economical point of view, large production of geopolymer activated by KOH and K₂SiO₃ will be more expensive compared to those activated by NaOH and Na₂SiO₃. However, it is well known that the photocatalytic action of TiO₂ is efficient in the presence of K⁺ ions, so the functionality of the matrices under study take advantage to the economic aspect. Halloysite (Al₂Si₂O₅(OH)₄·2H₂O) is a natural and abundant clayey material. It has the same theoretical chemical composition as kaolinite except that it contains additional water molecules between the layers and most commonly has a tubular morphology [20, 21]. On the contrary, kaolinite (Al₂Si₂O₅(OH)₄) is a simple layer aluminosilicate consisting of alternate layers of silica and alumina in tetrahedral and octahedral coordination, respectively [22] and typically occurs in platy form. Thermal treatment of halloysite and kaolinite clays from 550 to 800 °C causes their dehydroxylation resulting respectively in meta-halloysite and meta-kaolinite formation, required for the geopolymer synthesis [5, 23]. However, the additional water content to halloysite with respect to kaolinite allows earlier decomposition and dehydroxylation conducting to meta-halloysite at lower temperature. Kaze et al. [24] showed that calcined halloysite at 600 °C is suitable for geopolymers with good mechanical properties and long-term durability. Zhang et al. [25] in their

investigation claimed that 700 °C appeared as optimal calcination temperature of halloysite-clay that insured high strength. Recently, Tchakounté et al. [26] produced geopolymer binder from calcined halloysite and kaolinite clays at 700 °C, consolidated with sodium alkaline solution. The authors found that the obtained geopolymer binders made of calcined halloysite developed dense structure and high strength compared to that of metakaolin. This was due to fine particles of calcined halloysite that easily dissolve in alkaline solution producing a high quantity of the binder phase.

The main target of the present work was to evaluate and compare the influence of the addition of titanium dioxide in anatase form and rutile form, at different concentration, on the physical and mechanical properties of meta-halloysite based geopolymer. Before geopolymerization, the TiO₂ is added at various amount into aluminosilicate and the mix is calcined. The microstructural properties of the hardened products and the pore sizes distribution within the geopolymer composite were determined using Environment Scanning Electron Microscopy (ESEM) and Mercury Intrusion Porosity (MIP) respectively. In this first part of study, we focus on the influence of TiO₂ (anatase and rutile form) on the microstructure, porosity, densification and physico-chemical properties.

2 Materials and methods

2.1 Materials

Halloysite clay was collected from Balengou, a locality situated in the West Region of Cameroon. The physicochemical characterization of clay from Balengou was already studied by Kaze et al. [24]. They found that the main phases are Halloysite (Al₂Si₂O₅(OH)), Quartz (SiO₂), Hematite (Fe₂O₃) and Anatase (TiO₂). High purity analytical anatase and rutile (provided by a ceramic industry, Modena, Italy) were used as an additive. The commercial potassium silicate, namely Ksil 385 (K₂O/SiO₂ superior to 2.6), was provided by Ingessil s.r.l. Verona (Italy). Its chemical composition presents 9.11 wt% of K₂O, 26.45 wt% of SiO₂ and 64.44 wt% of H₂O. The potassium hydroxide was prepared from dried KOH (pellets; 85% purity), supplied by Labkem, Barcelona, Spain. Tap water was used as a solvent.

The fine aggregates (fine sand) used in this study were natural sand obtained from white kaolin. Kaolin is soaked in water for 24 h until it settled out. Then, kaolin is washed several times to separate the gravel and sand fraction from the silt and clay fraction. Sand was dried in the oven at 105 °C for 24 h. The dried sand was then completely sieved at 200 µm to remove gravel and others particles.

2.2 Methods

2.2.1 Preparation of solid precursors

The as-received clay from Balengou was oven-dried at 105 °C for 24 h to remove moisture. The dried clay was crushed in a mortar and then completely sieved at 200 µm.

The titanium dioxide (anatase or rutile) was added and uniformly mixed into the halloysite clay at four different contents (0%, 2.5%, 5%, 7.5% and 10%). Each formulation was calcined at 700 °C in a programmable electric furnace (MGS s.r.l., Italy) for 4 h with a heating and cooling rate of 5 °C min⁻¹. After calcination, each sample was left to cool freely in the furnace. The resulting powder was kept in a container to avoid its contact with air. The specimens are labelled MHA2.5, MHA5, MHA7.5 and MHA10 for samples containing anatase and MHR2.5, MHR5, MHR7.5 and MHR10 for samples containing rutile. MH samples without TiO₂ (the reference) is used for comparison.

2.2.2 Preparation of the alkali-silicate activator

The alkaline solution used was a mixture of required amounts of potassium silicate and aqueous solution of potassium hydroxide (10 M). The silica modulus (Ms) or molar ratio of SiO₂/K₂O and H₂O/K₂O were fixed at 1.55 and 13.27, respectively [27, 28]. This solution was prepared 1 h before use to enable equilibration and cooling.

2.2.3 Preparation of the geopolymer mortars

Geopolymer pastes were obtained by mixing suitable proportion of solid precursor and alkaline solution. The liquid/solid mass ratio for all specimens was kept constant at 0.65 to allow good workability of the paste. The mortars were obtained by mixing the slurry with aggregate (fine sand) at a mass ratio (precursors-to-aggregate) of 1:1.

The fresh geopolymer mortar samples were rapidly cast and full filling into molds of dimension 22 × 22 × 8 mm³. The molded specimens were vibrated for 5 min to ensure well distribution and to remove entrapped air bubbles. Then, they are compacted and covered with a thin film to prevent moisture loss during the setting. The geopolymer mortars were left in sealed plastic at room temperature for 24 h before demolded and then storing at room temperature until mechanical tested at 28-days (Fig. 1a). The mix design of the different compositions was labelled GMHA2.5, GMHA5, GMHA7.5, GMHA10 for geopolymers mixed with anatase (GMHA series), GMHR2.5, GMHR5, GMHR7.5 and GMHR10 for geopolymers combined with rutile (GMHR series) and GMH for the reference.

2.3 Characterization techniques

2.3.1 X-ray diffraction (XRD)

The X-Ray Diffraction data was collected using a Phillips Analytical X-Ray instrument (PW3710) operating with a CuKα, Ni-filtered radiation source (the wavelength was 1.5418 Å) and using a current of 40 mA and an acceleration Voltage of 40 kV. The XRD patterns were recorded in the range of 5° to 70°, with a scanning rate of 2 s per step.

2.3.2 Fourier transformed infra-red spectroscopy (FTIR)

Fourier Transformed Infra-Red Spectroscopy (Avatar 330 FT-IR, Thermo Nicolet) was performed on selected samples analyzing surface and bulk areas. A minimum of 32 scans between 4000 and 400 cm⁻¹ was averaged for each spectrum with 1 cm⁻¹ resolution.

2.3.3 Three-point flexural strength

The flexural strength of the geopolymer samples was measured in three-point bending configuration according to ASTM C 1161 – 02c standard [29], using a universal mechanical testing machine, type MTS 810, (MTS Systems Corporation, Eden Prairie, MN, USA). The strength of each specimens calculated as follow:

$$S = \frac{3 PL}{2 bd^2} \quad (1)$$

where S is strength (MPa), P the maximum applied load indicated by the testing machine (N), L span length (mm), b average width of specimen (mm) and d average thickness of specimen.

In our specific test configuration, b = 23 mm and d = 23 mm. The reported results were the average of four samples.

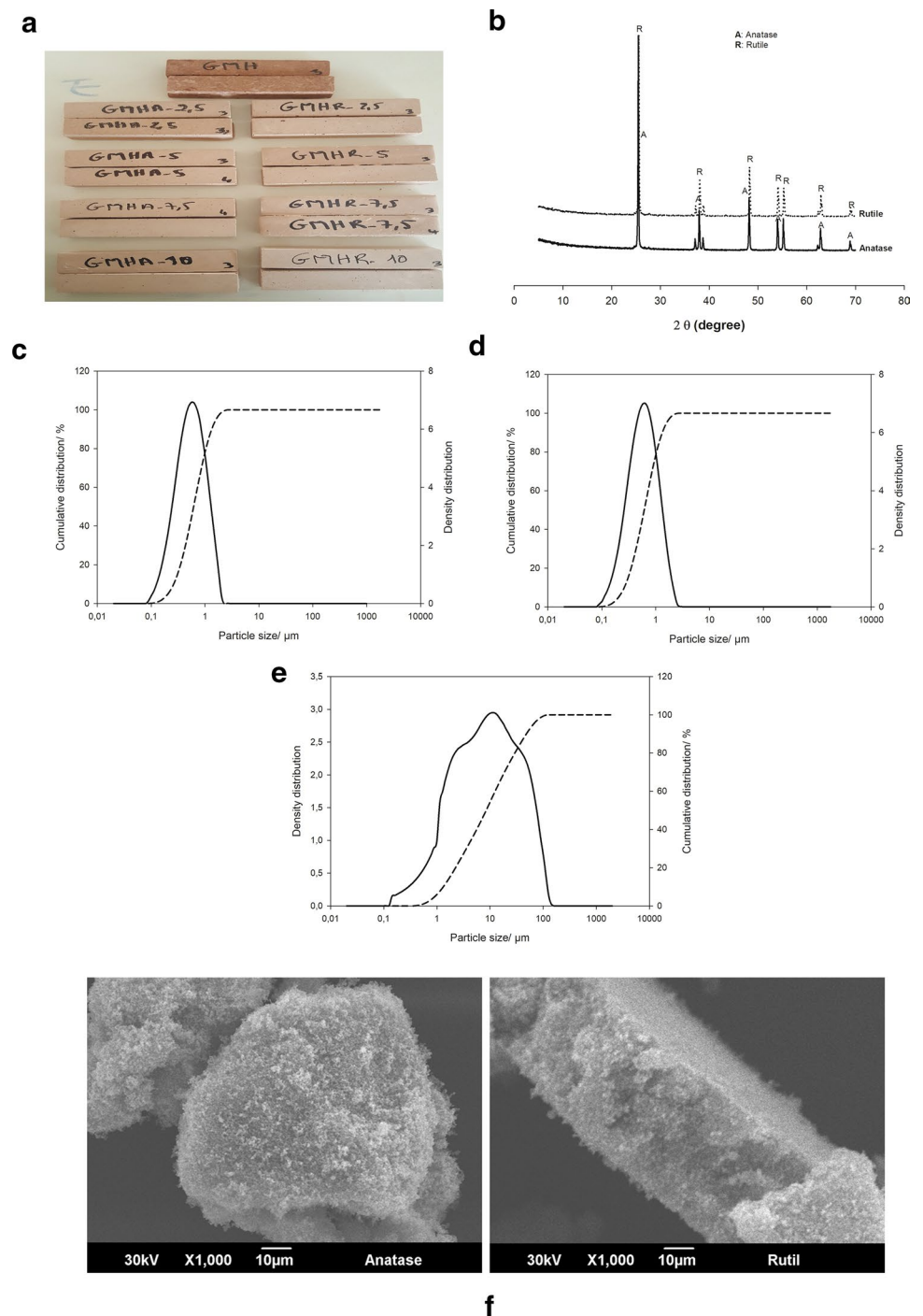
2.3.4 Water absorption, bulk density and apparent porosity

The Water absorption (Wa) analysis was conducted by immersing the specimen in water at ambient temperature for 24 h and comparing the Wet Weight (Ww) to the Dry Weight (Dw) according to Eq. (2):

$$Wa(\%) = \frac{(Ww - Dw)}{Dw} \times 100 \quad (2)$$

Bulk density and apparent porosity of the geopolymer samples were determined following the ASTM standard C373-88 (2006) using an analytical balance (Gibertini-Italy)

Fig. 1 **a** Photograph of geopolymer samples, **b** XRD analysis of anatase and rutile, **c** particle size distribution of anatase, **d** particle size distribution of rutile, **e** particle size distribution of halloysite, **f** SEM image of Ti_2O particles



with ± 0.0001 g sensitivity. Five representative test specimens were used to evaluate the mean values and standard deviation.

2.3.5 Environmental scanning electron microscopy (ESEM)

The ESEM analysis (Model Quanta 200, FEI, and Hillsboro, OR, USA) was performed at low vacuum on fractured

pieces collected from mechanical test. The specimens were preliminarily gold coated with 10 nm thick gold layer.

2.3.6 Mercury intrusion porosity (MIP)

The MIP constituted by an Autopore IV 9500, 33000 psia (228 MPa) covering the pore diameter range from approximately 20–0.001 μm having two low-pressure ports and one high-pressure chamber was used for the pore's

analysis. Pieces collected from the mechanical test were used to prepare specimens of $\sim 1 \text{ cm}^3$ of volume for the MIP.

3 Results and discussion

3.1 Characterization of the solid precursors

The Diffractogram of anatase and rutile is shown in Fig. 1b. The peaks located at approximately 25° , 38° , 48° , 55° and 63° 2θ were identified as Anatase (TiO_2 , ICCD 86-1157) or Rutile (TiO_2 , ICCD 001-1292). The high level of purity of anatase and rutile is confirmed by the intensity of the peak located at 25° 2θ .

Figure 1c–e and Table 1 present the physical properties of the solid precursors. The main diameters D_{10} , D_{50} and D_{90} are 0.26, 0.61 and $1.33 \mu\text{m}$ for Rutile, 0.25, 0.58 and $1.24 \mu\text{m}$ for Anatase, and 1.30, 8.32 and $49.20 \mu\text{m}$ for Halloysite. Their corresponding BET specific surface area are 10.52 ± 0.18 , 10.45 ± 0.10 and $27.92 \pm 0.12 \text{ m}^2 \text{ g}^{-1}$ for Rutile, Anatase and Meta-halloysite, respectively. From Fig. 1c–e, it is observed that anatase and rutile appear as nano materials with particles ranged between 0.12 – $2.23 \mu\text{m}$ and 0.12 – $2.75 \mu\text{m}$, respectively. In case of meta-halloysite, the particle size ranged between 0.12 and $146 \mu\text{m}$ contains more than 60% of particles with size $\leq 10 \mu\text{m}$. With this class of particles size distribution for both anatase and rutile, the insertion of these minerals' compounds could be expected during the meta-halloysite based geopolymer synthesis. More details in both anatase and rutile forms using Scanning Electron Microscope (SEM) are presented in Fig. 1f. It is observed that anatase particles exhibited circular morphology while rutile was tubular form. Therefore, these shapes for both nano compounds could likely influence the microstructural and mechanical properties of the end products.

Figure 2a presents the XRD patterns of meta-halloysite (MH) and various mixtures. It shows a typical broad hump appearing between 18° and 30° 2θ . The presence of this diffuse halo implies the predominance of amorphous phase in the meta-halloysite, which is suitable for the geopolymerization. Besides, there are few reflexion peaks

of crystalline phases like Quartz (SiO_2 , ICCD 46-1045), Muscovite ($\text{KAl}_2(\text{Si}_3\text{Al})\text{O}_{10}(\text{OH})_2$, ICCD 33-664), Hematite (Fe_2O_3 , ICCD 33-664), Halloysite ($\text{Al}_2\text{Si}_2\text{O}_5(\text{OH})_4 \cdot 2\text{H}_2\text{O}$) and Anatase (TiO_2 , ICCD 86-1157). For the meta-halloysite blended with TiO_2 at different concentration (Fig. 2a), the same crystalline phases were observed. The intensity of anatase increased with the increase of the percentage of TiO_2 addition in the solid precursors. The different phases of meta-halloysite (MH) and anatase are easily identified. It seemed that there were no new formed phases after calcination indicating that anatase did not react with meta-halloysite constituents.

Anatase and rutile presented very similar features at FTIR spectrum (Fig. 2b): principal bands are located at 670 and 668 cm^{-1} for anatase and rutile respectively. In Fig. 2c, the wavenumber of 1049.48 cm^{-1} is attributed to the asymmetric vibration modes of Si–O–Si and Si–O–Al bonds, which corroborates the aluminosilicate character of this MH [30]. The absorption band at 776.87 cm^{-1} is ascribed to the bending vibration of Si–O–Si and could be related to the presence of the amorphous silica contained in the structure of MH [31]. This is in accordance with the presence of dump observed in the XRD pattern (Fig. 2a) of MH. In fact, the calcination of halloysite produced meta-halloysite and amorphous silica. Residual quartz present in this meta-halloysite is confirmed by the signal at 776 cm^{-1} according to Tchakouté et al. [22]. At about 615.85 cm^{-1} , the smallest band is attributed to the bending vibration mode of O–Si–O [32]. The peaks that appear at 2324.23 and 2359.62 cm^{-1} are assigned to the absorption band of the sample holder. The bands at 3693.82 cm^{-1} , 3623.86 cm^{-1} and 1641.58 cm^{-1} are ascribed to the axial asymmetric and symmetric (bending and stretching) vibration mode of the hydroxyls OH associated to Al atoms and free water [24]. These bands disappeared after calcination indicating complete dehydroxylation of halloysite clay.

For the FTIR spectra of MH mixed with anatase (0, 2.5, 5.0, 7.5 and 10%) (Fig. 2d, e), a new peak that appeared near 693.28 cm^{-1} is ascribed to the Ti–O–Ti stretching of the anatase phase comparatively to the spectrum of MH [15]. This band relative to TiO_2 can be distinguished from those belonging to the meta-halloysite phases, which is in accordance with the observation made with XRD patterns. This band appeared at 699.6 cm^{-1} in the FTIR spectra of MH mixed with rutile.

3.2 Characterization of hardened products

3.2.1 Visual aspect of geopolymer specimens

The end products aged of 28 days are presented in Fig. 1a. It appears that the geopolymer mortars made without TiO_2 conserved the dark brown colour of meta-halloysite.

Table 1 Physical properties of raw materials

Raw materials	Particle size distribution (μm)			B.E.T specific surface area ($\text{m}^2 \text{ g}^{-1}$)
	D_{10}	D_{50}	D_{90}	
Rutile	0.261	0.613	1.328	10.52 ± 0.08
Anatase	0.244	0.577	1.242	10.45 ± 0.10
Halloysite	1.30	8.32	49.20	27.92 ± 10

Fig. 2 **a** XRD analysis of raw mixtures, **b** FTIR spectrum of anatase and rutile, **c** FTIR spectrum of halloysite and meta-halloysite, **d** FTIR spectrum of raw mixtures (MH with anatase), **e** FTIR spectrum of raw mixtures (MH with rutile)

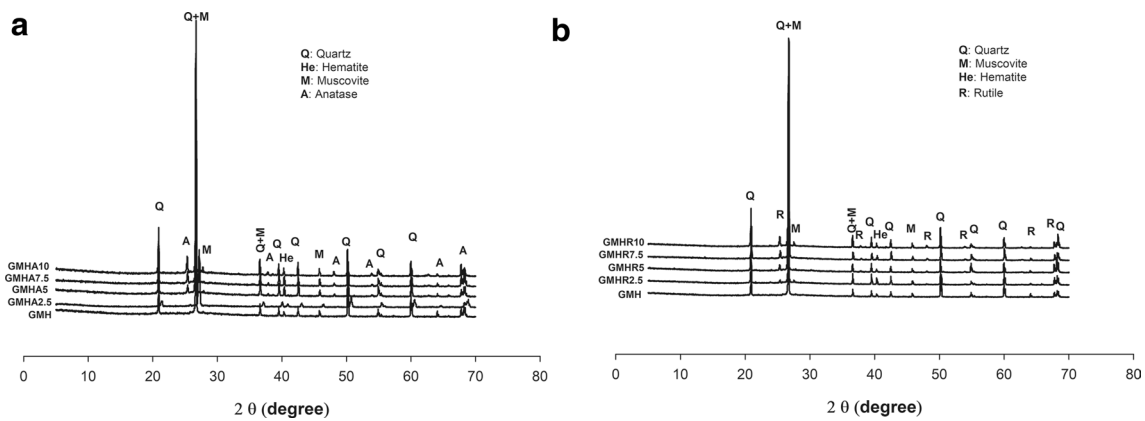
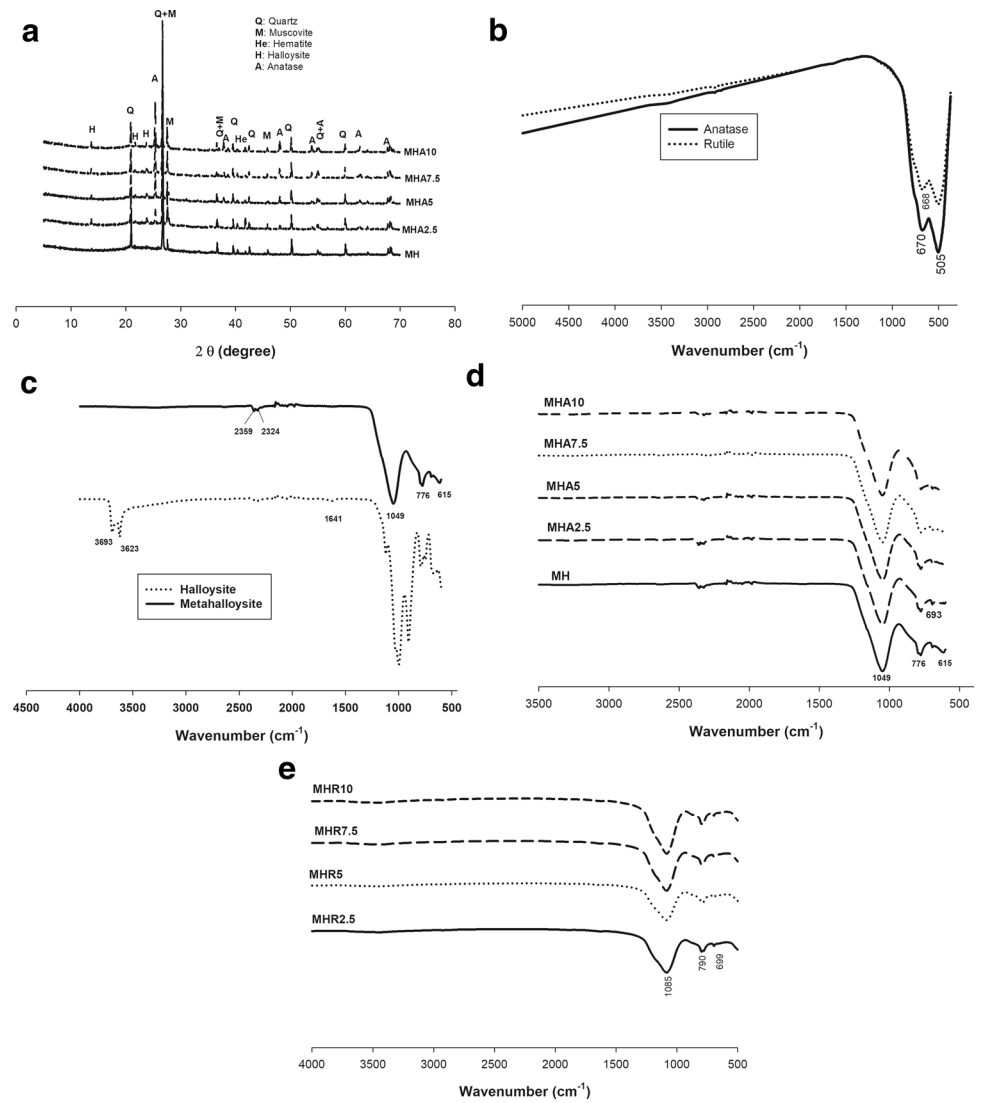


Fig. 3 XRD patterns of geopolymer mortars with additives: **a** anatase, **b** rutile

However, the addition of titanium dioxide reduces the darkness of the geopolymer mortars. The lightening of the color increases with the increase of the TiO_2 content. The amount of TiO_2 increases the color intensity of the geopolymer mortars from clear brown to dark brown.

3.2.2 Phases evolution

The Diffractograms of geopolymer mortars with TiO_2 addition are given in Fig. 3. The XRD patterns revealed the presence of quartz as the major crystalline phase. Apart from the quartz which comes from the sand added, there is the residual quartz from halloysite clay. Muscovite, hematite and anatase appeared as secondary phases. The presence of Muscovite, hematite and anatase in the geopolymer composite suggests that those minerals were not involved during the geopolymerization process and remained unaffected. TiO_2 is also inert and chemically stable. Beside the crystalline phases, the broad hump structure initially between 18° and $30^\circ 2\theta$, was shifted towards higher values of (2θ). This slight displacement of the dome now located at the 22° – $35^\circ (2^\circ)$ indicated the formation of a new amorphous phase, although the sand addition, which is fingerprint of geopolymer network [22, 30].

The absorption band, which initially appears at 1049.48 cm^{-1} in the FTIR spectrum of MH (Fig. 2c), is shifted to low wavenumbers in the range of 993 – 975 cm^{-1} and 1003 – 979 cm^{-1} for GMHA and GMHR geopolymer series respectively. The shift of this characteristic broad band at low wavenumber confirmed the dissolution of the meta-halloysite and the formation of the geopolymer gel [23]. From literature, this band is often used to determine the degree of polycondensation [32, 33]. The wavenumbers of the aforementioned broad band are slightly lower on the FTIR spectrum of GMHA series (Fig. 4a) compared to those of GMHR series

(Fig. 4b). This phenomenon could be attributed to the significant interaction between the MH and TiO_2 during the dissolution and polycondensation. This interaction conducted to the formation of highly cross-linking geopolymer framework in GMHA series. Moreover, according to Lee and van Deventer [34], the displacement of this characteristic band toward a lower wavenumber indicates that the original silicate or aluminosilicate structure had been significantly depolymerized.

The less intense peak of Ti–O–Ti bond is overlapped in the broad bands around 692 – 667 cm^{-1} and 688 – 665 cm^{-1} by the band ascribed to the Si–O stretching and deformation vibration for GMHA and GMHR series respectively. For the reference (GMH), the broad absorption bands at 3404 cm^{-1} and 1655 cm^{-1} are respectively attributed to vibration bending and stretching mode of the hydroxyl O–H bonds belonging to water molecules present on absorbed surface or entrapped in the 3D polymeric structure cavities during the geopolymerization process [35]. These bands are located in the range 3385 – 3355 cm^{-1} and 1649 – 1625 cm^{-1} for GMHA series (Fig. 4a), and in the range 3380 – 3349 cm^{-1} and 1639 – 1616 cm^{-1} for GMHR series (Fig. 4b). The intensity of these bands decreases with the proportion of the TiO_2 . This suggests the decrease in OH intensity with increasing of TiO_2 content, which results to the reduction of the silanol (Si–O–H) species and the formation of Si–O–Ti species on the geopolymer. The shift of the principal band toward lower wavenumber is due to the formation of Ti–O–H species resulting in the partial replacement of the tetrahedral Si sites with Ti following the change in the local chemical environment [36]. This trend is also similar to the studies reported by Guzmán-Aponte et al. [15] which related that the increase of TiO_2 additive content leads to an increase in the hydrophobicity of the material, i.e. its capacity to repel water.

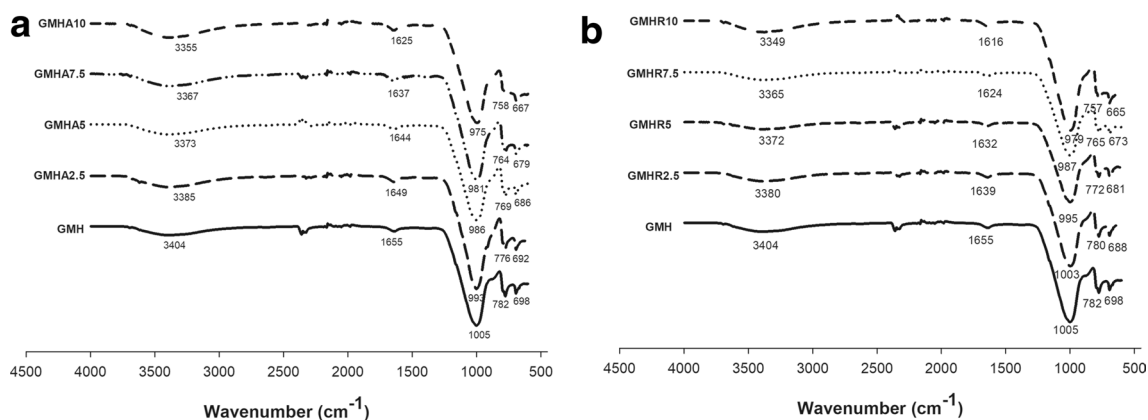


Fig. 4 FTIR spectra of geopolymer mortars with additives: **a** anatase, **b** rutile

Table 2 Water absorption, apparent porosity and bulk density data of the hardened samples

Samples	Water absorption (%)	SD/±	Apparent porosity (%)	SD/±	Bulk density (g cm ⁻³)	SD/±
GMH	14.2	0.2	34.5	2	1.8	0.02
GMHA2.5	14.13	0.1	34.46	1	1.81	0.02
GMHA5	14	0.1	33.4	3	1.79	0.01
GMHA7.5	13.4	0.3	32.2	1	1.81	0.03
GMHA10	12.4	0.2	30.01	2	1.86	0.01
GMHR2.5	12.42	0.2	29.48	1	1.83	0.01
GMHR5	12.54	0.3	30.6	2	1.87	0.01
GMHR7.5	12.4	0.2	29.9	1	1.85	0.03
GMHR10	16.5	0.4	39.6	1	1.72	0.02

3.2.3 Physico-mechanical properties

The variation of the water absorption, apparent porosity and bulk density of geopolymer mortars are recorded in Table 2. The addition of anatase decreased the water absorption from 14.2 to 12.4. This value is obtained with rutile right at 2.5 wt% and this value of water absorption is stable up to 7.5 wt%. Further increase in rutile content (> 7.5%wt) increased the water absorption, as the consequence of the increase of the apparent porosity (39.6 instead of 29.9). With the GMHA series, the apparent porosity decreased progressively and reached 30.01 only when 10% of anatase is added. The presence of TiO₂ species improved the dissolution, favoured the high degree of polycondensation and contributed to the densification of the geopolymer matrix by reducing the pores and voids. Besides, the values of density slightly increase with the content of TiO₂ as a result of pores filling. The high values of water absorption and apparent porosity of GMHR10 can suggest that more pores and voids are present in the structure of this geopolymer matrix due to the remaining

unreacted TiO₂ and other particles which can leach out of geopolymer matrix when the samples are immersed in water. Thereby, GMHR10 exhibits the lowest density value. This phenomenon can be explained by the presence in excess of TiO₂ particles in the geopolymer gel. These results are consistent with the trend of the flexural strength and the microstructure.

Figure 5 presents the 28-days mechanical strength behaviour of the hardened products made with the TiO₂ addition. The flexural strength values are 6.90, 7.98, 8.09, 8.40 and 9.13 MPa for GMHA series and 9.60, 11.30, 12.33, 11.20 MPa for GMHR series containing 0%, 2.5%, 5%, 7.5% and 10% amount of anatase or rutile, respectively. It can be seen that the flexural strength of geopolymer mortars is enhanced by increasing the rate of TiO₂ from 0 to 7.5%. This trend could be attributed to the TiO₂ particles which act as fillers or micro aggregates by reinforcing the geopolymer matrices resulting in compact and dense structure. This increase in flexural strength is in agreement with fine particles and morphological shapes of both anatase and rutile which can integrated the nano pore of geopolymer

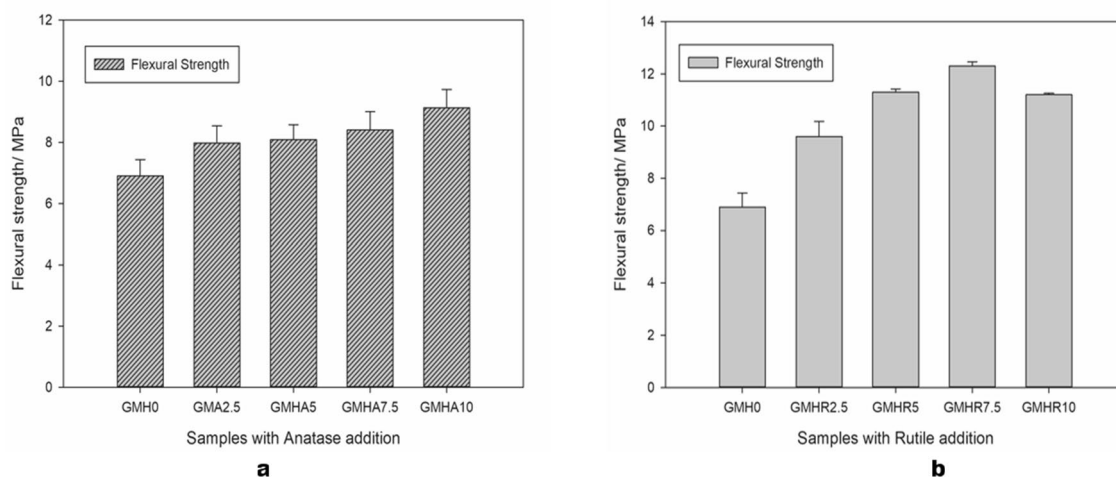


Fig. 5 Flexural strength of hardened samples with additives: **a** anatase, **b** rutile

leading to densification and compactness of structure. Above 7.5% of additive, it is noticed slightly decrease in flexural strength for GMHR series (from 12.33 to 11.20 MPa) while GMHA series show opposite tendency (from 8.40 to 9.13 MPa). The slight decrease could be justified by the fact that the binding phases were not still enough to embed

different particles within matrix which results in lower cohesion (Fig. 4b). It is noteworthy that GMHR series are stronger than those of GMHA. This also matches with morphological form of rutile which appears finer and presents high specific surface area. Hence in alkaline it could well behave compared to the later.

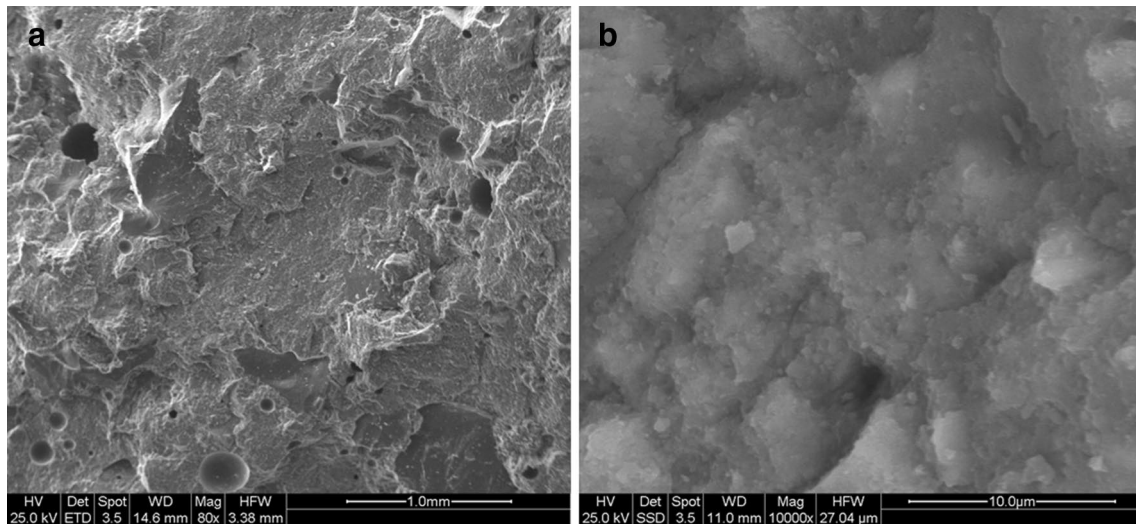


Fig. 6 Micrograph of the reference geopolymer sample (GMH): **a** at low magnification, **b** at high magnification

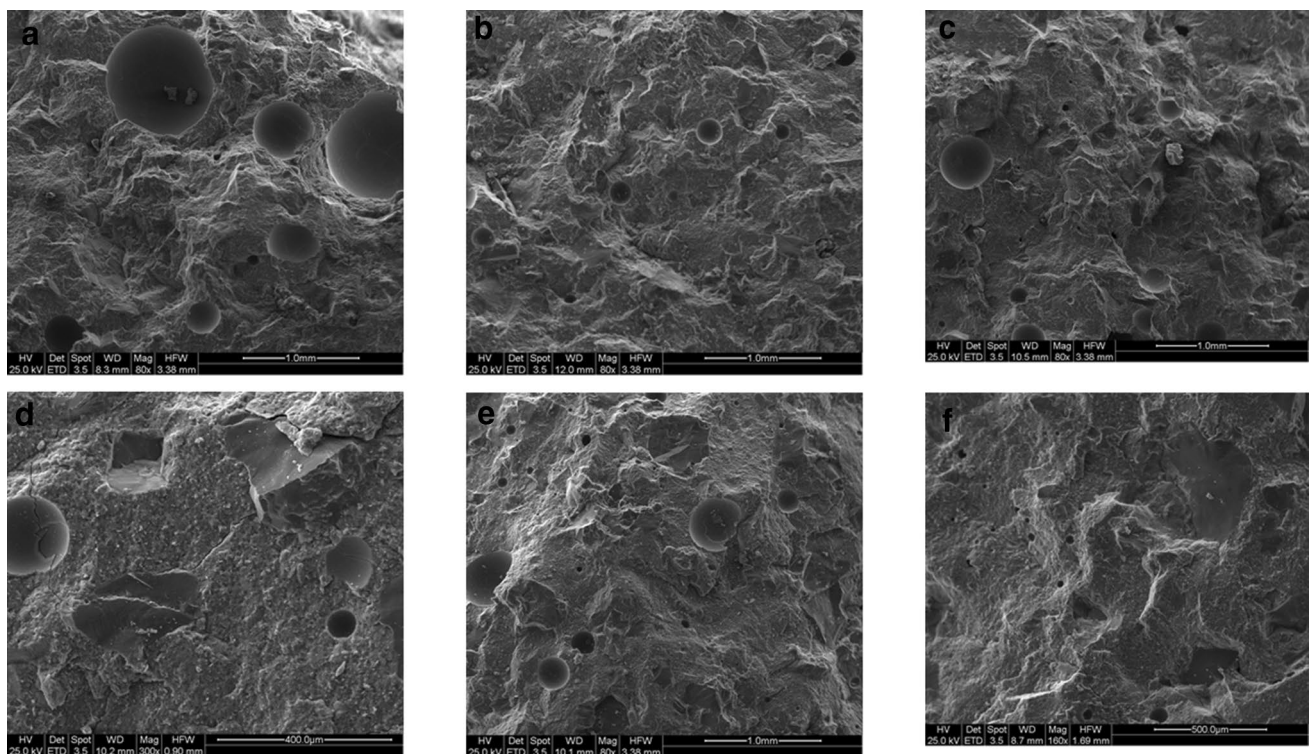


Fig. 7 Micrographs of the geopolymer mortars with TiO_2 addition at low magnification: anatase (**a–c** for 2.5, 5 and 7.5 wt% respectively), rutile (**d–f** for 2.5, 5 and 7.5 wt% respectively)

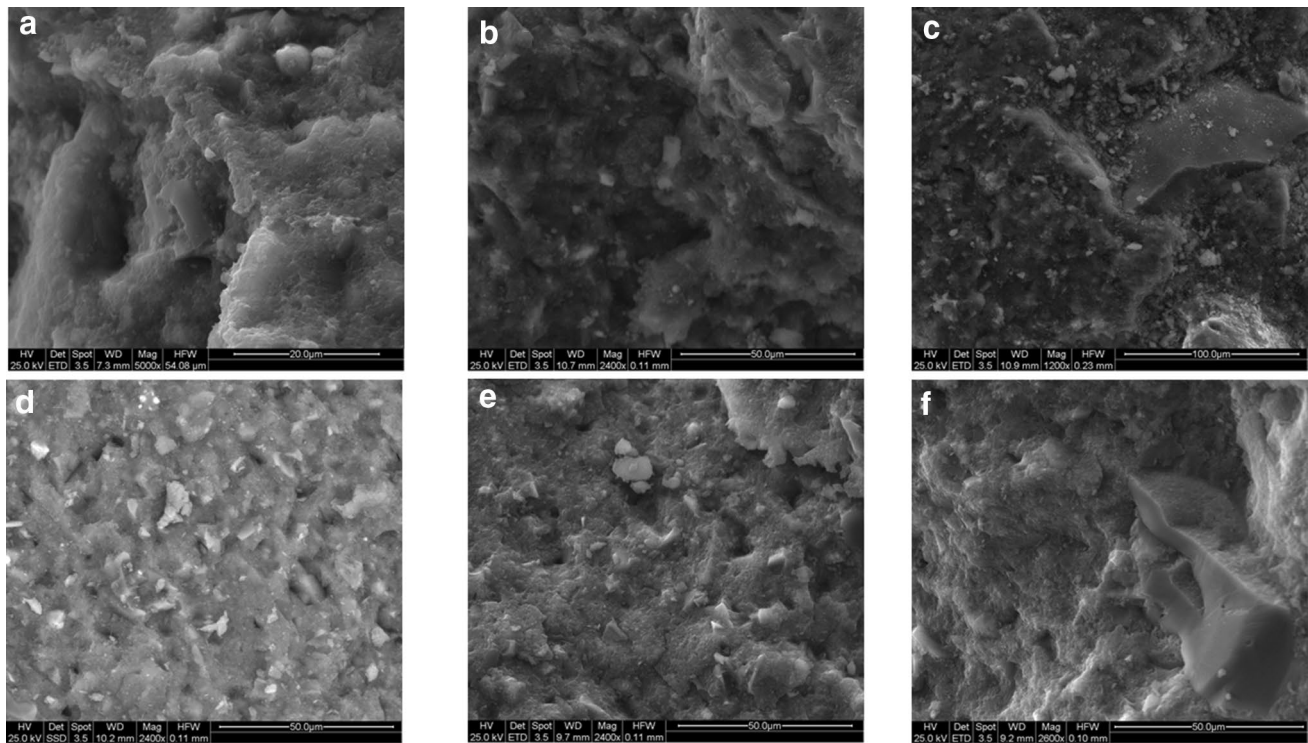


Fig. 8 Micrographs of the geopolymer mortars with TiO_2 addition at high magnification: anatase (**a–c** for 2.5, 5 and 7.5 wt% respectively), rutile (**d–f** for 2.5, 5 and 7.5 wt% respectively)

3.2.4 Microstructure

The SEM micrographs and the morphology features of geopolymer with various TiO_2 content up to 7.5% are summarized in Figs. 6, 7, 8. At low magnification ($\times 80$), both the geopolymer series exhibited a dense and homogeneous matrix with good compactness. In addition, there are no cracks appearance suggesting that the binder phase was enough to embed different particles within the matrix avoiding the Interfacial Zone (ITZ Formation) [37]. The geopolymer binder, with its grey tone, can be easily identified in all the micrographs. The presence of dispersed larger capillary pores is generally attributed to air bubbles that remain entrapped into the structure during the dissolution and polycondensation process [24, 38]. Compared to the micrograph of the reference mortar (Fig. 6), the number of pores and voids decreased with increasing the content of TiO_2 . This implies that the TiO_2 compounds (due to their interesting characteristics described in Fig. 1c, d) could have easily hook into the geopolymer network or act as a pore refining agent in the resulting matrix. The densification is enhanced with the presence of titanium particles which fill up the pore and voids space around them. They act as a nanofiller in the geopolymer matrix, which contributed to reinforce their structure. As consequence, the geopolymer matrix become more compact and denser.

The variation of the densification is in good agreement with the result of the flexural strength. Moreover, the particles of TiO_2 owing to their fineness and high BET surface, have the ability to replace silanol or voids. This is consistent with the results of IR spectrum of geopolymers which highlighted the formation of Si–O–Ti and Ti–O–H species due to the interaction between Si–OH and reactive TiO_2 units. These phenomena promote porosity refinement and enhance dense microstructure. Consequently, the flexural strength of the geopolymers was related to their microstructure, with the denser, less porous and finer textured samples being the strongest. Although the fact that both matrices appear dense and compact with TiO_2 , it is observed that the micrographs of GMHR series (Fig. 7d–f) are more homogeneous compared to GMHA series (Fig. 7a–c). The difference in both synthesized samples could be due to the following hypothesis: (1) More particles of TiO_2 in rutile form could have participated in geopolymerization reaction resulting in high extension of geopolymer binder. High polycondensation or polymerization justifies the high strength gained on these samples; (2) TiO_2 in anatase form is more crystalline, therefore would no integrate efficiently the matrix and would act more as filler. At high magnification ($\times 2400$), the reference matrix (Fig. 6) is less dense compared to the matrices with TiO_2 . Increasing the concentration of TiO_2 , the morphology

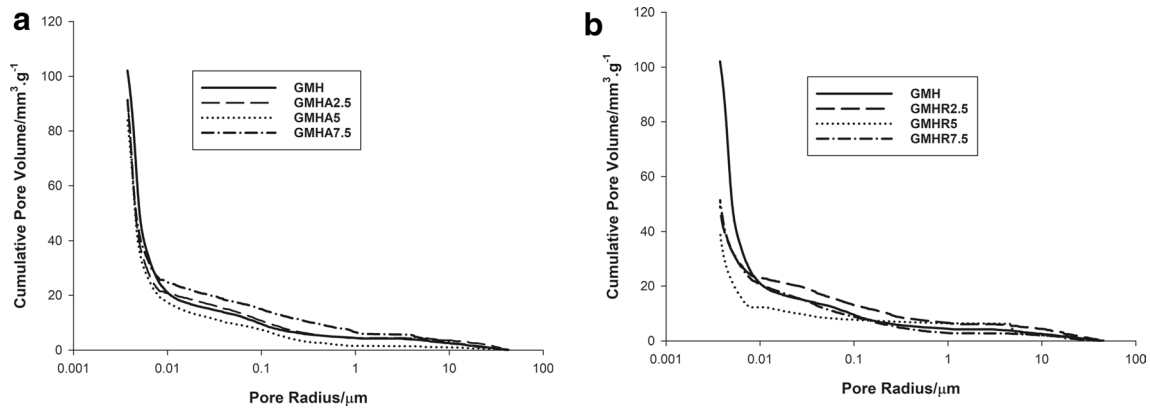


Fig. 9 Cumulative pore volume of the geopolymer samples with additives: **a** anatase and **b** rutile

Table 3 Variation of average pore radius and specific pore area of the geopolymer mortars

Samples	Total cumulative pore volume (mm ³ g ⁻¹)	Total surface area (m ² g ⁻¹)	Average pore radius (μm)
GMH	102.64	34.13	0.004
GMHA2.5	90.64	31.15	0.004
GMHA5	84.19	29.50	0.004
GMHA7.5	91.73	30.1	0.004
GMHR2.5	49.01	11.68	0.004
GMHR5	39.77	12.26	0.004
GMHR7.5	51.30	13.69	0.004

of the gel, which is smooth in GMH reference, develop progressively a coarsening microstructure. The matrix is viewed as a dense and well-packed particle of quartz sand, titanium dioxide and unreacted meta-halloysite, where the binding phase is not enough to completely embed the different particles within the matrix. Grains of quartz (dark grey particles) are now visible. Voids and spaces formation are the result of water evaporation which initially occupied round -cavities within geopolymer pastes. The coarsening microstructure of geopolymer matrices

containing the TiO₂ present, as evidence by the Mercury Intrusion Porosity (MIP), nanometric and micrometric porosities (Fig. 9). The cumulative pore volume of GMH is 102.2 mm³ g⁻¹. Increasing the rutile content (from 0 to 7.5%), it is noticed a significant decrease of the cumulative pore volume from 102.2 to 51.3 mm³ g⁻¹ (Fig. 9a). This as the results of filling mechanism of the pores and voids by rutile acting as strengthening agent which densified the geopolymer matrices. Their average radius of pores (Table 3) is closely 0.0041 μm. In the case of anatase, the cumulative pore volume slightly decreases from 102.2 to 84.2 mm³ g⁻¹ (Fig. 9b). The high values of the cumulative pore volume recorded in GMHA series showed that rutile particles are more efficient to reinforce geopolymer compared to anatase, this in agreement with the mechanical strength behavior (Fig. 5) and microstructure (Figs. 6, 7, 8). Finally, the use of nano particles of rutile and anatase in this study due to their high specific surface area and fine particles acted as a nuclei site by accelerating hydration phenomenon and promoting more geopolymer binder formation leading to the densification of the microstructure, thereby reducing the pore and void formation justifying the low porosity and water absorption [39].

Table 4 Pore size classification of the tested geopolymer matrices

Samples	Micropores (%) (< 1.25) nm	Mesopores (%) (1.25–25) nm	Macropores (%) (25–5000) nm	Voids (%) (5000–50,000) nm
GMH	–	65.25	27.12	7.6
GMHA2.5	–	83.76	10.26	5.98
GMHA5	–	83.2	13.3	3.5
GMHA7.5	–	75.40	18.03	6.56
GMHR2.5	–	58.77	23.68	17.54
GMHR5	–	73.3	11.5	15.2
GMHR7.5	–	67.80	23.73	8.47

Table 4 lists the classification of pores in the tested geopolymer matrices. The reference geopolymers (GMH) presents 7.6% of voids, 27.12% of macropores and 65.25% of mesopores. The addition of anatase make decrease the percentage of voids down to 3.5% where the macropores drops at 13.03%. In the meantime, the volume of mesopores increased from 65.25 to 83.2%. It should be noticed that after 5% of TiO_2 , the tendency is the increase of the voids and macropores with the reduction of mesopores (Table 4). When the TiO_2 is rutile, similar trend is observed. The limited reduction of macropores in this case reduces slightly the volume of mesopores. It can be concluded that the difference in flexural strength of the geopolymer composites is not only linked to the porosity and the pore size distribution, but also to the specific volume of the cross-linking bond developed during the geopolymerization. cross-linking which is more significant in composite with rutile compared to those with anatase.

The development of high volume of cross-linking bond in the geopolymer network with TiO_2 added contributes to the chemical stability of the geopolymer phases formed. Additionally, TiO_2 significantly improve the densification with important reduction of the porosity. The combine fixations of the highly cross-linking bonding phases and the improvement of the densification is positive for the long-term durability of the geopolymer matrices. In fact, the efficiency of the photocatalytic action of a matrix is not only linked to the chemical activities of TiO_2 linking to the destruction of NO_x , SO_x and others, the barrier that constitutive the well dense and compact matrix should ameliorate the action of TiO_2 since in the absence of porosity, the fixation of NO_x , SO_x and others is difficult.

4 Conclusion

Titanium dioxide in anatase and rutile form were used in various proportion as functional additive to halloysite clay. The obtained solid precursors were mixed with alkaline solutions to produce geopolymer mortars. The effect of adding TiO_2 on the physical, mechanical and microstructural properties of geopolymer composites was investigated. Flexural strength, water absorption, bulk density and microstructures were assessed and the results are summarized as follows:

1. Significant interactions were noticed between TiO_2 and meta-halloysite during geopolymerization, improving dissolution, polycondensation and densification of the geopolymer network. This enhancement is more obvious when rutile is used;
2. The flexural strength of geopolymer mortars were enhanced with the increase of TiO_2 concentration up to 7.5 wt%;
3. The number of pores and voids decreased with increasing content of the TiO_2 particles which contributes to produce more densified geopolymer structures. Moreover, titanium species were seemed to efficiently integrate the network structure geopolymer changing the morphology of the gel from smooth to coarser;
4. The refining of pore structure, the densification of the geopolymer matrix, which result to the improvement of flexural strength, could be attributed to the filling and replacement effects of TiO_2 .
5. The addition of rutile or anatase is found to be more effective as a means to improve the mechanical and microstructural properties of meta-halloysite based geopolymers. Thus, TiO_2 in both forms appears as catalyst for geopolymer reaction by extending the geopolymer binder within the matrix.

From the above-mentioned investigations, it appears that adding titanium dioxide (TiO_2 in anatase and rutile form) can be used successfully for the improvement of the mechanical and microstructural properties of geopolymer mortars. The best results are obtained with rutile form. TiO_2 in rutile form seem to have more participation in the geopolymerization reaction, resulting in high extension of geopolymer binder, which favors the high polycondensation. Results significant for the long-term durability of the geopolymer matrices.

Acknowledgements The authors of this article wish to acknowledge the FLAIR Fellowship African Academic of Science and the Royal Society. No. FLR/R1/201402. They also recognize the assistance of the staff of the Ceramics & Glass Laboratory of the University of Trento-Italy in the characterization of samples.

Compliance with ethical standards

Conflict of interest The authors declare that they have no conflict of interest.

References

1. Desarnaud E, Ando S, Desbarbieux T, Perbay Y (2006) Changement Climatique, les enjeux du développement durable au sein de l'industrie du ciment: réduction des émissions de CO_2 , p 45
2. Davidovits J (2011) Geopolymer chemistry and applications, terminology, 3rd edn. Institute Geopolymer, Saint-Quentin, p 612p
3. Duxson P, Fernández-Jiménez A, Provis JL, Lukey GC, Palomo A, van Deventer JSJ (2007) Geopolymer technology: the current state of the art. *J Mater Sci* 42:2917–2933
4. Bakharev T (2005) Resistance of geopolymer materials to acid attack. *Cem Concr Res* 35:658–670

5. Elimbi A, Tchakoute HK, Njopwouo D (2011) Effects of calcination temperature of kaolinite clays on the properties of geopolymer cements. *Constr Build Mater* 25:2805–2812
6. Kamseu E, Leonelli C, Perera DS, Melo UC, Lemougna PN (2009) Investigation of volcanic ash based geopolymers as potential building materials. *Inter Ceram* 58:136–140
7. Rodriguez ED, Bernal SA, Provis JL, Paya J, Monzo JM (2013) Effect of nanosilica-based activators on the performance of an alkali-activated fly ash binder. *Cem Concr Compos* 35:1–11
8. Paul SC, van Rooyen AS, van Zijl GPAG, Petrik LF (2019) Properties of cement-based composites using nanoparticles: a comprehensive review. *Constr Build Mater* 189:1019–1034
9. Pelaez M, Nolan NT, Pillai SC, Seery MK, Falaras P, Kontos AG, Dunlop PSM, Hamilton JWW, Byrne JA, O'Shea K, Entezari MH, Dionysiou DD (2012) A review on the visible light active titanium dioxide photocatalysts for environmental applications. *Appl Catal B Environ* 125:331–339
10. Chen J, Poon CS (2009) Photocatalytic construction and building materials: from fundamentals to applications. *Build Environ* 44:1899–1906
11. Fischer K, Gawel A, Rosen D, Krause M, Latif AA, Griebel J, Prager A, Schulze A (2017) Low temperature synthesis of anatase/rutile/brookite TiO₂ nanoparticles on a polymer membrane for photocatalysis. *Catalyst* 7:209
12. Strini A, Roviello G, Ricciotti L, Ferone C, Messina F, Schiavi L, Corsaro D, Cioffi R (2016) TiO₂-based photocatalytic geopolymers for nitric oxide degradation. *Materials* 9:513
13. Seo D, Yun TS (2017) NO_x removal rate of photocatalytic cementitious materials with TiO₂ in wet condition. *Build Environ* 112:233–240
14. Janus M, Madraszewski S, Zajac K, Kusiak-Nejman E, Morawski AW, Stephan D (2019) Photocatalytic activity and mechanical properties of cements modified with TiO₂/N. *Materials* 12:3756
15. Guzmán-Aponte LA, de Gutiérrez RM, Maury-Ramírez A (2017) Metakaolin-based geopolymer with added TiO₂ particles: physico-mechanical characteristics. *Coatings* 7:233
16. Duan P, Yan C, Luo W, Zhou W (2016) Effect of adding nano-TiO₂ on compressive strength, drying shrinkage, carbonation and microstructure of fluidized bed fly ash based geopolymer paste. *Constr Build Mater* 106:115–125
17. Zheng K, Chen L, Gbozee M (2016) Thermal stability of geopolymers used as supporting materials for TiO₂ coating through sol-gel process: feasibility and improvement. *Constr Build Mater* 125:1114–1126
18. Duxson P, Lukey GC, van Deventer JSJ (2006) Thermal evolution of metakaolin geopolymers: part 1—physical evolution. *J Non-Cryst Solids* 352(s52–53):5541–5555
19. Lemougna PN, Wand KT, Tang Q, Melo UC, Cui XM (2016) Recent developments on inorganic polymers synthesis and applications. *Ceram Int* 42:15142–15159
20. Lecomte-Nana G, Goure-Doubi H, Smith A, Wattiaux A, Lecomte G (2012) Effect of iron phase on the strengthening of lateritic-based “geomimetic” materials. *Appl Clay Sci* 70:14–21
21. Bayiha BN, Billong N, Yamb E, Kaze RC, Nzengwa R (2019) Effect of limestone dosages on some properties of geopolymer from thermally activated halloysite. *Constr Build Mater* 217:28–35
22. Tchakoute HK, Rüscher CH, Djobo JNY, Kenne BBD, Njopwouo D (2015) Influence of gibbsite and quartz in kaolin on the properties of metakaolin-based geopolymer cements. *Appl Clay Sci* 107:188–194
23. Kaze CR, Venyete P, Nana A, Deutou JN, Tchakoute HK, Rahier H, Kamseu E, Melo UC, Leonelli C (2019) Meta-halloysite to improve compactness in iron-rich laterite-based alkali activated materials. *Mater Chem Phys* 44:18499–18508
24. Kaze CR, Tchakoute HK, Mbakop TT, Mache JR, Kamseu E, Melo UC, Leonelli C, Rahier H (2018) Synthesis and properties of inorganic polymers (geopolymers) derived from Cameroon-meta-halloysite. *Ceram Int* 44:18499–18508
25. Zhang B, Guo H, Yuan P, Li Y, Wang Q, Deng L (2020) Geopolymerization of halloysite via alkali-activation: dependence of microstructures on precalcination. *Appl Clay Sci*. <https://doi.org/10.1016/j.clay.2019.105375>
26. Tchakoute HK, Melele SJK, Djamen AT, Kaze CR, Kamseu E, Nansheu CNP, Leonelli C, Rüscher CH (2020) Microstructural and mechanical properties of poly(sialate-siloxo) networks obtained using metakaolins from kaolin and halloysite as aluminosilicate sources: a comparative study. *Appl Clay Sci* 186:105–448
27. Khale D, Chaudhary R (2007) Mechanism of geopolymerisation and factors influencing its development: a review. *J Mater Sci* 42:729–746
28. Tippayasam C, Balyore P, Thavorniti P, Kamseu E, Leonelli C, Chindaprasit P, Chaysuwan D (2016) Potassium alkali concentration and heat treatment affected metakaolin-based geopolymer. *Constr Build Mater* 104:293–297
29. ASTM C 1161 – 02c (2002) Standard test method for flexural strength of advanced ceramics at ambient temperature
30. Tchakoute HK, Rüscher CH, Kamseu E, Andreola F, Leonelli C (2018) Influence of the molar concentration of phosphoric acid solution on the properties of metakaolin-phosphate-based geopolymer cements. *Appl Clay Sci* 147:184–194
31. Bewa CN, Tchakoute HK, Fotio D, Rüscher CH, Kamseu E, Leonelli C (2018) Water resistance and thermal behavior of metakaolin-phosphate-based geopolymer cements. *J Asian Ceram Soc* 6:3
32. Chindaprasit P, Jaturapitakul C, Chalee W, Rattanasak U (2009) Comparative study on the characteristics of fly ash and bottom ash geopolymers. *Waste Manag* 29:539–543
33. Gao K, Lin KL, Hwang CL, Shiu HS, Chang YM, Cheng TW (2014) Effects SiO₂/Na₂O molar ratio on mechanical properties and the microstructure of nano-SiO₂ metakaolin-based geopolymers. *Constr Build Mater* 53:503–510
34. Lee WKL, van Deventer JSJ (2003) Use of infrared spectroscopy to study geopolymerization of heterogeneous amorphous aluminosilicates. *Langmuir* 19:8726–8734
35. Beleuk à Mougam LM, Mohamed H, Kamseu E, Billong N, Melo UC (2017) Properties of geopolymers made from fired clay bricks wastes and rice husk ash (RHA)-sodium hydroxide (NaOH) activator. *Mater Sci Appl* 8:537–552
36. Yu DE, Bravo PI, Shimizu E, Malenab RA, Tigue AA, Dela Cerna KM, Janairo JI, Promentilla MA (2019) Nanocrystalline titania coated metakaolin and rice hull ash based geopolymer spheres for photocatalytic degradation of dyes in wastewater. *Orient J Chem* 35(1):167–172
37. Tchadjé LN, Djobo JNY, Ranjbar N, Kenne BBD, Elimbi A, Njopwouo D (2016) Potential of using granite waste as raw material for geopolymer synthesis. *Ceram Int* 42:3046–3055
38. Kamseu E, Nait-Ali B, Bignozzi MC, Leonelli C, Rossignol S, Smith DS (2012) Bulk composition and microstructure dependence of effective thermal conductivity of porous inorganic polymer cements. *J Eur Ceram Soc* 32(8):1593–1603
39. Shaikh FUA, Supit SWM (2014) Mechanical and durability properties of high volume fly ash (HVFA) concrete containing calcium carbonate (CaCO₃) nanoparticles. *Constr Build Mater* 70:309–321

Publisher's Note Springer Nature remains neutral with regard to jurisdictional claims in published maps and institutional affiliations.